Direct observations of CO2 emission reductions due to COVID-19 lockdown across European urban districts

Nicolini, Giacomo

2022-07-15

Nicolini , G , Antoniella , G , Carotenuto , F , Christen , A , Ciais , P , Feigenwinter , C , Gioli , B , Stagakis , S , Velasco , E , Vogt , R , Ward , H C , Barlow , J , Chrysoulakis , N , Duce , P , Graus , M , Helfter , C , Heusinkveld , B , Järvi , L , Karl , T , Marras , S , Masson , V , Matthews , B , Meier , F , Nemitz , E , Sabbatini , S , Scherer , D , Schume , H , Sirca , C , Steeneveld , G-J , Vagnoli , C , Wang , Y , Zaldei , A , Zheng , B & Papale , D 2022 , ' Direct observations of CO2 emission reductions due to COVID-19 lockdown across European urban districts ' , Science of the Total Environment , vol. 830 , 154662 . https://doi.org/10.1016/j.scitotenv.2022.1546

http://hdl.handle.net/10138/348210
https://doi.org/10.1016/j.scitotenv.2022.154662

Science of the Total Environment 830 (2022) 154662

Contents lists available at ScienceDirect

Science of the Total Environment

journal homepage: www.elsevier.com/locate/scitotenv

Direct observations of CO_2 emission reductions due to COVID-19 lockdown across European urban districts

Giacomo Nicolini [a,b,*], Gabriele Antoniella [a,b], Federico Carotenuto [c], Andreas Christen [d], Philippe Ciais [e], Christian Feigenwinter [f], Beniamino Gioli [c], Stavros Stagakis [f,g], Erik Velasco [h], Roland Vogt [f], Helen C. Ward [i], Janet Barlow [j], Nektarios Chrysoulakis [g], Pierpaolo Duce [c], Martin Graus [i], Carole Helfter [k], Bert Heusinkveld [l], Leena Järvi [m,n], Thomas Karl [i], Serena Marras [a,o], Valéry Masson [p], Bradley Matthews [q,r], Fred Meier [s], Eiko Nemitz [k], Simone Sabbatini [a,b], Dieter Scherer [s], Helmut Schume [q], Costantino Sirca [a,o], Gert-Jan Steeneveld [l], Carolina Vagnoli [c], Yilong Wang [t], Alessandro Zaldei [c], Bo Zheng [u], Dario Papale [a,b]

[a] Euro-Mediterranean Center on Climate Change, Italy
[b] DIBAF University of Tuscia, Italy
[c] CNR, National Research Council, Italy
[d] Environmental Meteorology, Institute of Earth and Environmental Sciences, University of Freiburg, Germany
[e] Laboratoire des Sciences du Climat et de l' Environnement, CEA CNRS UVSQ, C.E. Orme des Merisiers Gif sur Yvette, France
[f] University of Basel, Switzerland
[g] Institute of Applied and Computational Mathematics, Foundation for Research and Technology Hellas (FORTH), Greece
[h] Independent researcher, Singapore
[i] Dep. of Atmospheric and Cryospheric Sciences, University of Innsbruck, Austria
[j] Dep. of Meteorology, University of Reading, UK
[k] UK Center for Ecology & Hydrology, Penicuik, UK
[l] Wageningen University, Meteorology and Air Quality Section, Wageningen, Netherlands
[m] Institute for Atmospheric and Earth System Research, Helsinki, Finland
[n] Institute of Sustainability Science, Faculty of Science, University of Helsinki, Finland
[o] Dept. of Agricultural Sciences, University of Sassari, Italy
[p] University of Toulouse, Météo-France and CNRS, France
[q] University of Natural Resources and Life Sciences, Department of Forest- and Soil Sciences, Institute of Forest Ecology, Vienna, Austria
[r] Environment Agency Austria, Vienna, Austria
[s] Chair of Climatology, Institute of Ecology, Technische Universität Berlin, Germany
[t] Key Laboratory of Land Surface Pattern and Simulation, Institute of Geographic Sciences and Natural Resources Research, Chinese Academy of Sciences, Beijing, China
[u] Tsinghua Shenzhen International Graduate School, Tsinghua University, China

* Corresponding author at: Euro-Mediterranean Center on Climate Change, Italy.
E-mail address: giacomo.nicolini@cmcc.it (G. Nicolini).

http://dx.doi.org/10.1016/j.scitotenv.2022.154662

HIGHLIGHTS

- Following the outbreak of the COVID-19 pandemic in 2020, people's activities drastically changed due to mobility restrictions.
- This affected urban CO_2 emissions and we wanted to quantify its impact during the lockdown and in the following months.
- We analysed eddy covariance measurements of urban CO_2 fluxes over the lockdown in thirteen European city districts.
- Data provided the measured evidence of a consistent reduction of CO_2 emissions, proportional to the stringency of restrictions.
- The reduction was temporary in most of the city districts, as emissions rebounded to usual levels once restrictions were eased.

GRAPHICAL ABSTRACT

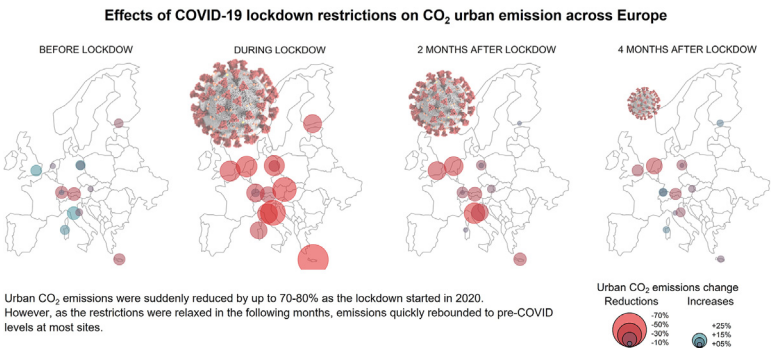

ARTICLE INFO

Article history:
Received 7 November 2021
Received in revised form 10 March 2022
Accepted 14 March 2022
Available online 19 March 2022

Editor: Jianmin Chen

Keywords:
Eddy-covariance
Urban fluxes
Urban pollution
Traffic emissions
Corona virus pandemic
Social restrictions

ABSTRACT

The measures taken to contain the spread of COVID-19 in 2020 included restrictions of people's mobility and reductions in economic activities. These drastic changes in daily life, enforced through national lockdowns, led to abrupt reductions of anthropogenic CO_2 emissions in urbanized areas all over the world. To examine the effect of social restrictions on local emissions of CO_2, we analysed district level CO_2 fluxes measured by the eddy-covariance technique from 13 stations in 11 European cities. The data span several years before the pandemic until October 2020 (six months after the pandemic began in Europe). All sites showed a reduction in CO_2 emissions during the national lockdowns. The magnitude of these reductions varies in time and space, from city to city as well as between different areas of the same city. We found that, during the first lockdowns, urban CO_2 emissions were cut with respect to the same period in previous years by 5% to 87% across the analysed districts, mainly as a result of limitations on mobility. However, as the restrictions were lifted in the following months, emissions quickly rebounded to their pre-COVID levels in the majority of sites.

1. Introduction

The large current reliance of urban energy use on fossil fuels makes cities the main contributors to global anthropogenic emissions of carbon dioxide (CO_2) (Oke et al., 2017). Urban CO_2 emissions, being linked to human needs and activities such as mobility, heating, and economic activities, are highly dynamic, varying substantially at sub-hourly, daily, weekly and seasonal time scales. Urban vegetation plays a role in the CO_2 exchange of urban areas with uptake and release of CO_2 also varying at multiple timescales in response to a range of controls (Ribeiro et al., 2019).

At the scale of large urban areas ($\approx$100 km^2), CO_2 flux budgets can be constrained indirectly by in situ and/or remote sensing measurements of CO_2 concentrations using atmospheric transport models as studied in e.g. Paris (Staufer et al., 2016) and Indianapolis (Turnbull et al., 2019). At similar or smaller scales, urban CO_2 fluxes can be estimated by combining building energy modules, bottom-up emission inventory models based on activity data and emission factors, and biogeochemical models for urban vegetation (Goret et al., 2019; Gurney et al., 2019). At the neighbourhood or district scale ($\approx$ 1 km^2), net CO_2 fluxes can be directly inferred from eddy-covariance (EC) measurements of turbulent CO_2 exchange.

EC has been widely used over natural ecosystems to investigate biosphere responses to environmental and biological factors (Baldocchi, 2014), while in urban ecosystems its application has grown steadily over the past 15 years (e.g. Helfter et al., 2016; Nordbo et al., 2012; Pérez-Ruiz et al., 2020; Roth et al., 2017; Salgueiro et al., 2020; Stagakis et al., 2019; Vogt et al., 2006; Ward et al., 2015). Urban EC measurements have been shown to be valuable for detecting short- and long-term changes in fluxes, and for studying the drivers of local CO_2 emissions and 'urban metabolism' leading to a better understanding of the carbon cycle in cities (Christen et al., 2011; Crawford et al., 2011; Feigenwinter et al., 2012; Velasco and Roth, 2010). The EC method is based on simultaneous high-frequency (e.g. 10–20 Hz) measurements of the vertical wind velocity and CO_2 concentration, or any other scalar entity such as heat, moisture, trace gases, and aerosols, allowing for the estimation of the vertical exchange of such scalars through turbulent motions (eddies) within the mean air flow. Conventionally, positive values represent upward fluxes, i.e. net emissions to the atmosphere, and negative values represent downward fluxes, i.e. net uptake by the underlying surface. Measurements are continuous and representative of a target source area (footprint) typically of the size of a city district (i.e. 10^4–10^8 m^2) depending on the measurement height with respect to average building height. For a complete description of the EC flux method see, for example, Aubinet et al. (2012).

The onset of the COVID-19 pandemic in Europe in early spring 2020, caused drastic changes to people's lives and socio-economic activity. The governmental actions taken to break the chain of disease transmission included the closure of schools and non-essential businesses, banning social gatherings, and enforcing home confinement. Such measures reduced mobility and economic activity, and inevitably impacted energy use and anthropogenic CO_2 emissions. It also displaced daytime populations from the work-place to residential areas, which likely impacted the spatial distribution of emissions associated with building energy use, as well as affecting emissions from transport. Assessments of national activity reductions combined with empirical relations to predict emissions suggested that CO_2 emissions of individual countries fell by up to 30% during the peak of the

lockdowns in spring 2020 (Forster et al., 2020; Le Quéré et al., 2020; Liu et al., 2020). Although associated CO_2 emissions reductions at the city scale are to be expected, the magnitude and variability of these reductions cannot be simply determined from national-level changes. Quantitative estimates of urban emission reductions due to COVID-19 restrictions based on atmospheric measurements have so far only been estimated for a few cities worldwide (Gualtieri et al., 2020; Lamprecht et al., 2020; Sugawara et al., 2021; Velasco, 2021; Yadav et al., 2021).

In this study we present CO_2 fluxes measured by a network of 13 EC stations in 11 European cities. These datasets span several years before the pandemic until October 2020. Urban EC stations operating before and during 2020 present a unique opportunity to investigate how the drastic perturbations in human activity caused by the COVID-19 pandemic have impacted local CO_2 emissions. CO_2 flux data at half-hourly resolution allows for temporal changes in CO_2 emissions to be tracked both during the initial lockdown period and during the subsequent recovery phase when economic activities and mobility gradually resumed.

Our analysis focuses on the following questions:

- Do direct flux measurements confirm the emissions reduction predicted by coarse-scale inventory models?
- What was the magnitude of the reduction in emissions at the district scale, and how does this vary from place to place?
- Were reductions in emissions related to the stringency of the restriction measures?
- Were there more substantial reductions for certain hours of the day or days of the week?
- Did emissions return to previous levels after the restrictions were lifted?
- Was this recovery dependent on urban features (e.g. land use type, density of the road network, amount of vegetation)?

2. Methods

Using micrometeorological data (Nicolini et al., 2022) from 13 urban EC stations in 11 cities across Europe (Table 1 and supplementary "Study sites" Section), we evaluated district-scale changes in urban CO_2 fluxes between 2020 and previous years. These changes were analysed in relation to the stringency of the local lockdown rules, taking into consideration the characteristics of each site in terms of local citizens activities (e.g. commuting, economic activities, domestic heating) and urban features.

Each EC station (Table 1) was equipped with a 3D ultrasonic anemometer, a gas analyser for measuring CO_2 concentrations, and meteorological sensors measuring air temperature and humidity, air pressure and solar radiation. All systems collected data at 10 or 20 Hz, which were processed by the researchers in charge of each station according to commonly accepted procedures (Aubinet et al., 2012) to obtain the half-hourly CO_2 fluxes used in the analysis. Data quality assurance was assessed by each group following standard quality control and filtering procedures, albeit with allowances for site-to-site variations (details can be found in the main references for each site which are given in Table 1). For this study, we additionally excluded CO_2 flux data beyond the physically plausible range of -50 to 200 μmol m^{-2} s^{-1}, those from wind sectors prone to flow disturbance by physical obstacles (e.g. measurement tower structure) and those outside a site-specific quantile range calculated over a 3 weeks moving window using the 0.5% and the 99.9% probability were excluded. This quantile range was taken asymmetrically because in urban environments sporadic large negative fluxes (sinks) are far less likely than large positive fluxes (emissions). Data were not gap-filled as it was not required for the type of analysis performed.

Flux observations from previous years up to and including 2019 were used as a reference to compare changes before, during, and after the lockdown periods with related restrictions that affected each city district. Pre-2020 records span between 2 and 14 years depending on the station (Table S1). We focused our analysis on four distinct periods defined following the Oxford COVID-19 Government Response Tracker (OxCGRT) Stringency Index (SI) (Hale et al., 2020a, 2020b). The SI quantifies policies that governments have taken to respond to the pandemic; it is calculated as the average of a set of macro-indicators of containment and closure policies including closure of schools, universities and workplaces, cancelling of public events, limits on private gatherings, shutting-down public transport, orders to "shelter-in-place" or otherwise confine to homes, restrictions on internal movement between cities/regions, and restrictions on international travel. The SI ranges between 0 (no restrictions) and 100 (maximum level of restrictions). Although the contributing factors to this index vary between countries and cities, the SI has been shown to provide global insight into the pandemic's evolution and implementation of measures (Cross et al., 2020). We set a minimum threshold of 65 (64.3 is the 60th quantile of the SI values for the analysed cities over the period January–October 2020) to define the lockdown period (LOCK) in each city. The length of this period (and the maximum value of SI reached) varied from 19 days in Helsinki to 75 days in Basel and Amsterdam (Table S2). Then,

Table 1
Summary of the cities and respective EC stations involved in the study. The *station ID* is the naming used in this analysis, containing the names of the respective cities, z is the measurement height (m), z/z_h is the ratio between z and mean building height (z_h).

Country	Station ID	Latitude	Longitude	Data range		z	z/zh	EC system	Main references
						m		sonic; IRGA	
Austria	AT-Innsbruck	47.26404	11.38571	2017-08-01	2020-10-31	42.8	2.5	CSAT3; EC155	Karl et al., 2020
Austria	AT-Vienna	48.18181	16.39088	2018-01-01	2020-10-01	144.0	7.0	WM Pro; LI-7500	Matthews and Schume, 2022
Switzerland	CH-Basel-A	47.55123	7.59560	2016-01-01	2020-10-19	41.0	2.5	CSAT3; LI-7500	Lietzke et al., 2015
Switzerland	CH-Basel-K	47.56173	7.58049	2016-01-01	2020-10-19	39.0	2.3	HS; LI-7500	Lietzke and Vogt, 2013
Germany	DE-Berlin ROTH	52.45723	13.31583	2018-06-01	2020-09-30	40.0	2.4	Irgason	Vulova et al., 2021
Germany	DE-Berlin TUCC	52.51228	13.32786	2014-07-03	2020-09-30	56.0	2.8	Irgason	Jin et al., 2020; Vulova et al., 2021
Finland	FI-Helsinki	60.20269	24.96231	2014-01-01	2020-09-30	31.0	1.6	USA-1; LI-7200	Järvi et al., 2012, Järvi et al., 2009
Greece	GR-Heraklion	35.33616	25.13282	2016-10-27	2020-09-30	27.0	2.4	Irgason	Stagakis et al., 2019
Italy	IT-Florence	43.77441	11.25511	2005–09–14	2020-10-22	33.0	1.3	81000V; LI-7500	Gioli et al., 2012; Matese et al., 2009
Italy	IT-Pesaro	43.91197	12.90404	2014-08-09	2020-10-20	23.0	1.5	WM Pro; LI-7500	Gioli et al., 2012; Matese et al., 2009
Italy	IT-Sassari	40.71695	8.57593	2016-01-01	2020-10-26	22.0	2.0	HS-50; LI-7200	not available
Netherlands	NL-Amsterdam	52.36654	4.89290	2018-05-01	2020-10-13	40.0	2.8	CSAT3; LI-7500	Steeneveld et al., 2020
United Kingdom	UK-London	51.52140	−0.13881	2011–09–15	2020-09-30	190.0	22.0	R3–50; LI-7500; P1301-f	Helfter et al., 2016, Helfter et al., 2011

EC system instruments: *CSAT3*, 3-D sonic anemometer (Campbell Scientific, Inc.); *EC155*, closed-path $CO2/H_2O$ gas analyser (Campbell Scientific, Inc.); *WM Pro*, WindMaster Pro 3-axis anemometer (Gill Instruments Limited); *LI-7500*, LI-7500 open path $CO2/H_2O$ analyser (LI-COR, Inc.); *HS-100*, HS-100 horizontal-head ultrasonic anemometer (Gill Instruments Limited); *Irgason*, Irgason integrated $CO2/H_2O$ open-path gas analyser and 3-D sonic anemometer; *USA-1*, USA-1 ultrasonic anemometer (METEK Meteorologische Messtechnik GmbH); *LI-7200*, LI-7200 enclosed-path $CO2/H_2O$ gas analyser (LI-COR, Inc.); *81000V*, 81000V ultrasonic anemometer (R. M. Young Company); *HS-100*, HS-100 horizontal-head ultrasonic anemometer (Gill Instruments Limited); *R3–50*, R3–50 3-axis anemometer (Gill Instruments Limited); *1301-f*, Picarro 1301-f flux CO_2, CH_4, and H_2O gas concentration analyser (Picarro, Inc.).

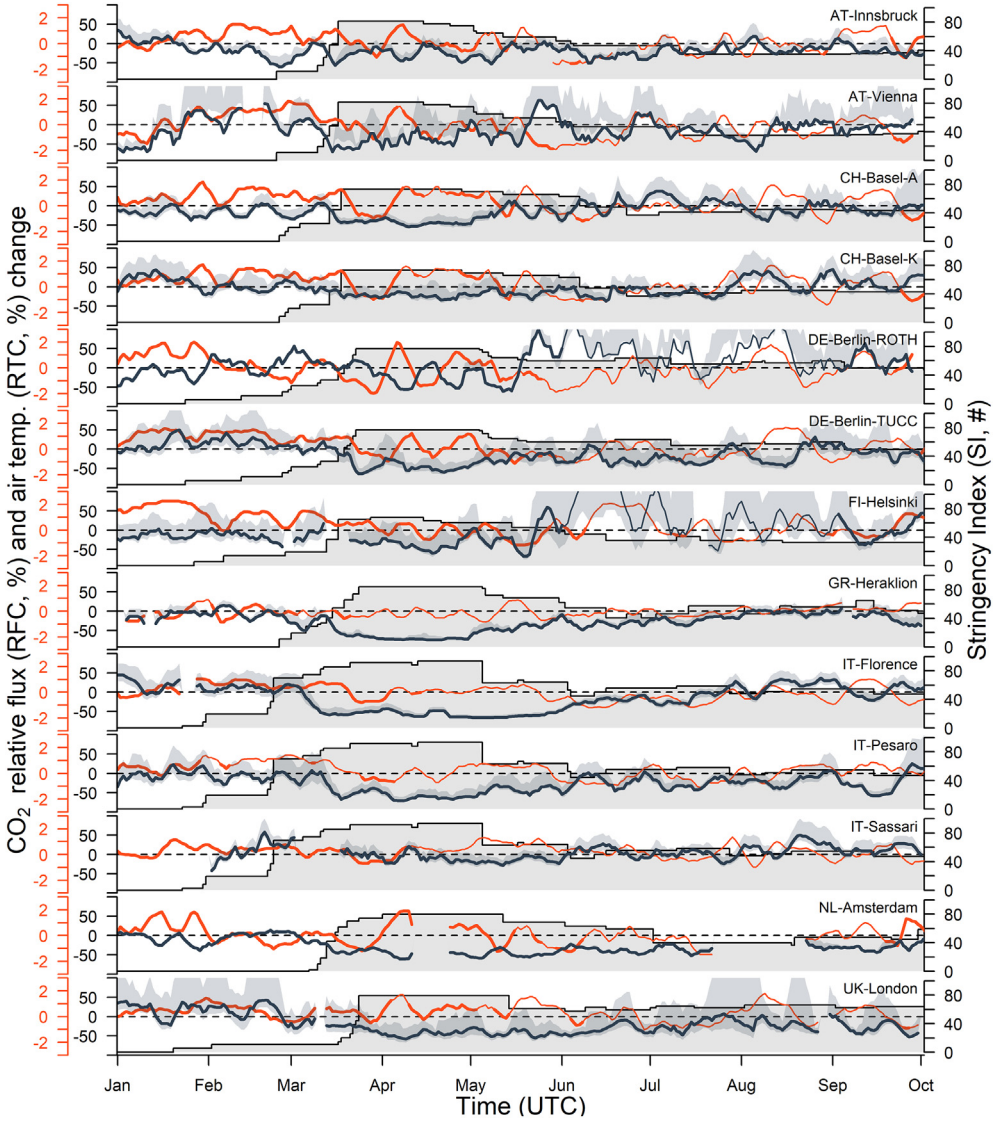

Fig. 1. Daily CO_2 relative flux change (*RFC*, %, dark grey line, left y-axis) for January to October 2020 relative to the average flux over previous years. Daily fluxes are computed as the median of half-hourly values and smoothed by a 7-day moving window average. Negative *RFC*s indicate emission reduction. The shaded area around the *RFC* curve represents the *RFC* interquartile range calculated using individual previous years as a baseline. The Oxford Stringency Index (SI, 0–100, light grey shaded area, right y-axis) illustrates country-wide levels of restrictions due to the COVID-19 pandemic. The thin line segments of the *RFC* curves for DE-Berlin-ROTH and FI-Helsinki indicate periods of relevant vegetation activity (assumed to be from June 1st to September 1st). Relative air temperature change (*RTC*, %, red curve, secondary left y-axis) is computed similarly to *RFC*, using daily average temperatures (in K). Bold *RTC* line sections highlight the days with air temperature < 15 °C assumed as a threshold for comfort temperature.

a pre-pandemic period (PRE) was defined lasting from January 1st to the beginning of the lockdown in each location, and two subsequent periods of 60 days each, POST1 and POST2, were identified after LOCK to evaluate the emissions recovery (Table S2).

The anomalies in CO_2 fluxes during each of these periods were quantified in terms of the relative flux changes (*RFC*, %) computed as:

$$RFC = \frac{x_{2020} - x_{base}}{|x_{base}|} \cdot 100 \quad (1)$$

where x_{2020} and x_{base} are the average fluxes observed for each period in 2020 and for the corresponding period in previous years (considered as the baseline period), respectively. The computation of *RFC* was based on daily means (Sections 3.1 and 3.2), diel cycles (Section 3.3) or half-hourly means of the CO_2 fluxes (Sections 3.4 and 3.5), depending on the context. Negative values of *RFC* indicate a reduction of the CO_2 fluxes with respect to the baseline period, while positive values are associated with increased CO_2 fluxes.

We also calculated the relative air temperature change in a similar way (*RTC, %*) to evaluate the potential effect of temperature anomalies on the observed fluxes. We assumed that CO_2 emissions from commercial and domestic heating become relevant when the daily mean air temperature is below 15 °C. This threshold is considered as the temperature at which heating in Europe is expected to be switched on (Matzarakis and Balafoutis, 2004; Pigeon et al., 2007).

Uncertainties in CO_2 flux averages, both daily and half-hourly in case of diel cycles, were calculated as the standard error over the single half-hourly values. Non-parametric statistical metrics (Spearman's rank correlation, Kruskal-Wallis test by rank and Wilcoxon rank-sum test) were performed to evaluate the significance of differences in the CO_2 fluxes, and the correlation of *RFC* with *RTC* and SI.

To evaluate the contributions to *RFC* from different land cover categories and emission sources within the footprint of each tower, CO_2 fluxes

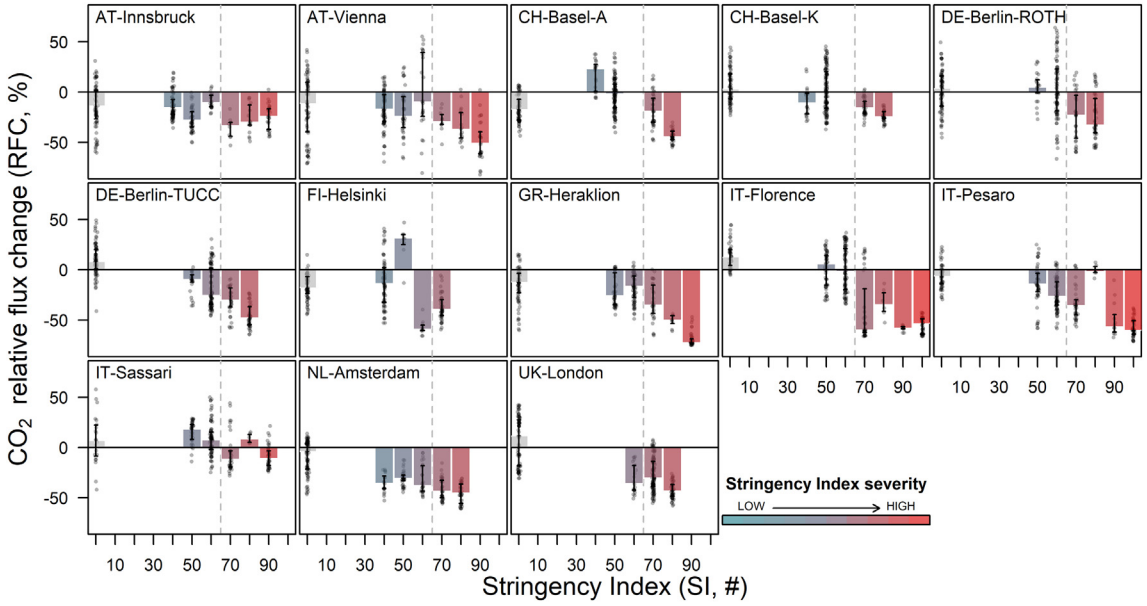

Fig. 2. CO_2 relative flux change (*RFC, %*) as a function of the Oxford stringency index (SI). Daily *RFC* values over the whole monitored period, smoothed over a 7-days moving window, are grouped by SI classes with a width of 10 points. The bars represent the median of daily *RFC* values, error bars represent their interquartile range, dots represent the individual *RFC* values, the colour gradient represents SI severity (low to high, blue to red). *RFC* data up to the first day of lockdown, or when SI < 20, are aggregated in the grey bar placed before the SI class 0–10 (left-most bar). The dashed vertical line represents the SI value we considered as the threshold for the most restrictive measures (i.e. 65). Days with CO_2 fluxes close to zero (± 1 μmol m^{-2} s^{-1}) were removed to avoid excessive noise in the ratio calculation of the *RFC*, without affecting the results.

were also analysed by wind sectors (see also the supplementary "Spatial analysis" Section). The land use and land cover (LULC) information was extracted from the European Urban Atlas (UA) 2012 database (Montero et al., 2014), cropping circular areas centred at each flux tower. The radii of these areas were set equal to the median distance of the 70th percentile of the estimated contribution of the cumulative flux footprint (Kljun et al., 2015), irrespective of wind direction. This length represents the distance within which 70% of the measured flux is estimated to originate. It was calculated for 8 sites at which footprint estimates were available whereas, for the other 5 sites, it was estimated according to an average ratio between the calculated distances and measurement heights (Table S1).

To facilitate the interpretation of results, similar UA-LULC classes were combined into broader classes, the main four of which were: (*i*) predominantly residential areas (RES), consisting mainly of residential structures, but also including downtown areas and city centres (higher storeys of buildings are mostly residential), with various degrees of soil sealing; (*ii*) non-residential areas (nRES), consisting in industrial and commercial areas, as well as schools and military units; (*iii*) areas dominated by roads and railway networks (ROD); and (*iv*) green urban areas (GUA), that include pervious surfaces with vegetation e.g. lawns, parks, greenbelts, farmland, urban forests. We used Google Earth Imagery (© 2020 Google), Sentinel-2 satellite Normalised Difference Vegetation Index (NDVI), and local knowledge of each site, to improve the characterization of districts. At each site, relatively homogeneous wind sectors were associated with single LULC class (supplementary "Spatial analysis" section). The NDVI data were used to determine the extent of green spaces and to track the temporal dynamics in vegetation activity, to minimise the risk of misinterpreting trends in *RFC* arising from year-to-year variations (supplementary "Vegetation analysis" section).

Two independent datasets of city-scale activity, the Carbon Monitor emission inventory (CM, https://carbonmonitor.org/) and Google COVID-19 Community Mobility Reports (©2021Google), were used to assist interpretation of the *RFC* at each site. We estimated CO_2 daily emissions from road transportation at the city scale for 2019 and 2020 following the CM methodology (Liu et al., 2020): a sigmoid function describing the relationship between daily mean congestion level (as reported by TomTom's traffic report, https://www.tomtom.com) and mean traffic volume data for the city of Paris was used as a proxy to estimate the road-traffic related CO_2 emissions from the other cities using the TomTom's reports for each city. Then, we compared the changes between measured and predicted emissions for residential and non-residential sectors with a substantial presence of roads (20% as minimum).

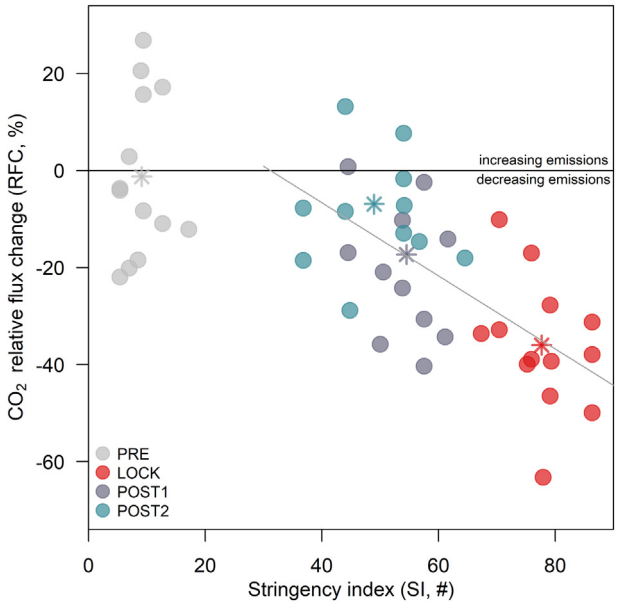

Fig. 3. Average CO_2 relative flux change (*RFC*, %) as a function of the average Oxford stringency index (SI) for each period. *RFC* values represent the average of daily *RFCs* obtained from the comparison of CO_2 daily fluxes in 2020 with those from all available previous years. Each dot represents the average *RFC* and SI for each period, in each city district. The considered periods are: the period from the beginning of 2020 up to the beginning of the first lockdown (PRE) when social restrictions were not present, the lockdown period (LOCK), and two subsequent periods of 60 days each after the end of the lockdown (POST1 and POST2). Stars represent the average *RFCs* and SIs across all the city districts. The *RFC*-SI linear regression (grey line) is fitted to the LOCK, POST1 and POST2 data points.

Table 2
CO_2 relative flux change (*RFC, %*), calculated as the average percentage change between 2020 and previous years CO_2 daily fluxes. Minimum (*min*) and maximum (*max*) *RFC*s are calculated over all available years (*Ny*, excluding the 2020 and years with no data for the period of concern). Average *RFC* values are those displayed in Fig. 3. *RFC* values are ranked by colours: from red to green going from higher emission reductions (negative *RFC*) to higher emission increases (positive *RFC*).

	PRE				LOCK				POST1				POST2			
station ID	RFC	min	max	Ny	RFC	min	max	Ny	RFC	min	max	Ny	RFC	min	max	Ny
AT-Innsbruck	-22	-25	-19	2	-28	-35	-20	2	-24	-27	-22	2	-12	-13	-11	2
AT-Vienna	-4	-13	5	2	-47	-50	-43	2	-10	-12	-8	2	-8	-12	-4	2
CH-Basel-A	-20	-25	-12	4	-33	-35	-29	4	1	-7	17	4	-8	-15	-3	4
CH-Basel-K	3	-1	7	4	-10	-20	-2	4	-17	-23	-2	4	13	9	20	4
DE-Berlin-ROTH	-11	-11	-11	1	-17	-17	-17	1	3	-5	11	2	-1	-3	0	2
DE-Berlin-TUCC	17	-2	33	5	-39	-52	-23	5	-14	-24	14	6	-15	-19	-8	6
FI-Helsinki	-12	-37	10	6	-34	-48	-21	5	1	-39	79	5	8	-33	34	6
GR-Heraklion	-18	-20	-16	2	-63	-63	-63	2	-21	-25	-15	3	-7	-12	-1	3
IT-Florence	27	-8	60	10	-38	-53	-32	9	-38	-51	-32	8	-2	-29	22	10
IT-Pesaro	-8	-15	8	5	-50	-54	-45	5	-31	-38	-16	4	-13	-21	-4	3
IT-Sassari	16	9	23	4	-31	-35	-23	4	-2	-8	7	4	8	-3	21	4
NL-Amsterdam	-4	-4	-4	1	-40	-46	-34	2	-36	-36	-36	2	-29	-30	-27	2
UK-London	21	1	68	6	-39	-51	-24	5	-34	-50	-12	6	-18	-51	48	6

Community mobility data released by Google during the pandemic (Google LLC., 2020) were used to track changes in people's mobility, specifically as a measure of the time spent by the population at places of residence. This data source has already been used to estimate changes in CO_2 emissions at the neighbourhood scale (Velasco, 2021). Mobility levels during the LOCK, POST1 and POST2 periods were compared to baseline mobility values calculated as median values of each day of the week over the five weeks between January 3rd and February 6th 2020.

3. Results

3.1. Reduction in daily CO_2 emissions during COVID-19 lockdown

For all sites, we found a clear reduction in CO_2 emissions coinciding with COVID-19 restrictions (Fig. 1), with daily *RFC* values mostly spanning between -%5 to −87%. Compared to the same period in previous years, the observed reduction during the LOCK period in which the most restrictive measures were applied, was statistically significant at all sites (Wilcoxon rank-sum test, $\alpha = 0.01$, supplementary Fig. S8). The largest reductions were seen at GR-Heraklion (*RFC* daily means interquartile range IQ = [−75%, −46%]), IT-Pesaro ([−71%, −34%]), IT-Florence ([−66%, −37%]), DE-Berlin-TUCC ([−63%, −36%]), UK-London ([−58%, −33%]) and CH-Basel-A ([−53%, −26%]). In some of the cities (AT-Vienna, GR-Heraklion, NL-Amsterdam, and UK-London), emissions started to decrease 5–7 days earlier than the start of the official lockdowns in response to initial mobility restrictions and recommendations to stay at home.

For most cities, the strictest lockdown measures were gradually reduced in early May (Fig. 1 and Table S2). For the post lockdown periods (POST1, POST2), daily CO_2 fluxes returned to levels similar to previous years in most of the city districts (DE-Berlin ROTH, GR-Heraklion, IT-Florence, IT-Sassari, CH-Basel-A, CH-Basel-K, AT-Innsbruck, AT-Vienna, FI-Helsinki). In the others CO_2 fluxes remained 13% to 30% below the baseline values.

The dynamics of the *RFC* roughly followed those of the SI at all sites, with stronger emission reductions (negative *RFC*) observed during more stringent confinement periods. Over the whole monitored period, the correlation between *RFC* and SI was statistically significant (see Table S7, Spearman ρ varying between −0.65 and −0.14, $p < 0.05$) except at DE-Berlin-ROTH and FI-Helsinki ($\rho = -0.12$, $p > 0.05$), both characterized by abundant vegetation cover (> 60% of the land cover, Figs. S3 and S4). The correlation became statistically significant at both sites however ($\rho = -0.18$ and −0.28, respectively, $p < 0.01$) when the analysis was done excluding the data collected during the vegetation growing season (approximately from June, thin lines in Fig. 1, see the Supplementary "Vegetation analysis" Section) that could have acted as a confounding factor.

Since the lockdown period began in early spring, CO_2 emissions from building heating contributed to total CO_2 fluxes at most sites. As a result, synoptic variations in weather patterns and associated temperature changes impact CO_2 emissions and are responsible for some of the variability in the *RFC*. For relatively cold days (mean air temperature < 15 °C) without strong restrictions (SI < 40), a negative correlation was found between *RFC* and *RTC,* in particular at CH-Basel-A, DE-Berlin-ROTH and NL-Amsterdam (Spearman ρ correlation coefficient between −0.33 and −0.44, $\alpha = 0.05$), probably due to a reduction in heating-related emissions. This aspect is further analysed in Section 3.3.

3.2. Relation between reduction of emissions and severity of restrictions

All cities had a significant reduction in emissions during the most restrictive measures (LOCK, SI > 65), and several cities also reported reduced emissions in the subsequent months (POST1 and POST2) during which some restrictive measures remained in place. The relation between *RFC* and SI is examined in more detail in Fig. 2 (the statistical significance is shown in Fig. S9). In almost all cities the *RFC* reached its minimum (<−50%) for the highest values (SI > 70–80), when the most restrictive measures were in place.

There were however two districts where emissions were only slightly reduced even under the most stringent restrictions (IT-Sassari and CH-Basel-K), suggesting that the main emission sources of those districts were partly decoupled from the lockdown severity, for example if the measured fluxes were not strongly affected by traffic reductions. Some cities showed a clear and consistent decrease in *RFC* with SI (e.g. AT-Vienna, GR-Heraklion, IT-Pessaro) while others show more variability (e.g. AT-Innsbruck, FI-Helsinki) hinting at a more complex situation in which other drivers contributed to the emission reductions (further detail in Section 3.3).

When analysing all districts together (Fig. 3), a consistent and significant correlation between *RFC* and SI was found (slope = −0.75, $p < 0.001$). The average *RFC* during the LOCK period across all sites was

Fig. 4. Diel patterns of CO_2 fluxes during the initial COVID-19 lockdown restrictions (LOCK), before (PRE), and afterward (POST1 and POST2). Fluxes measured in 2020 (red lines) and previous years (grey lines) are included for comparative purposes. Shaded areas represent the standard error of the mean of the individual half-hourly fluxes. The relative flux change (*RFC*) is reported as the average percentage change between 2020 and previous years. The individual daily patterns of previous years are presented in grey colours: dark grey 2019, and greyscale (direction dark to light) for 2018 and earlier. Average *RFC* values are those reported in Table 2.

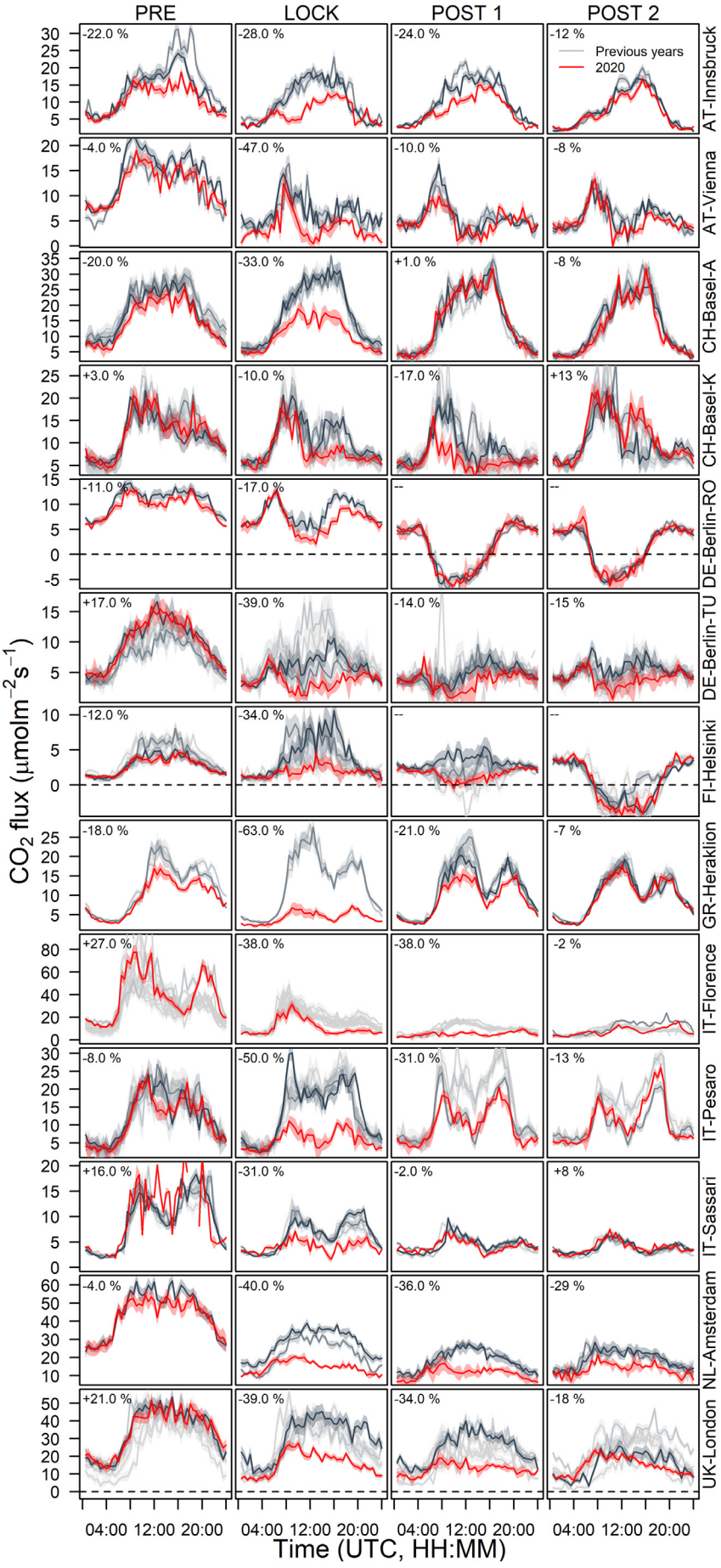
PRE
LOCK
POST 1
POST 2
Previous years
2020
AT-Innsbruck
AT-Vienna
CH-Basel-A
CH-Basel-K
DE-Berlin-RO
DE-Berlin-TU
FI-Helsinki
GR-Heraklion
IT-Florence
IT-Pesaro
IT-Sassari
NL-Amsterdam
UK-London
-22.0 %
-28.0 %
-24.0 %
-12 %
-4.0 %
-47.0 %
-10.0 %
-8 %
-20.0 %
-33.0 %
+1.0 %
-8 %
+3.0 %
-10.0 %
-17.0 %
+13 %
-11.0 %
-17.0 %
--
--
+17.0 %
-39.0 %
-14.0 %
-15 %
-12.0 %
-34.0 %
--
--
-18.0 %
-63.0 %
-21.0 %
-7 %
+27.0 %
-38.0 %
-38.0 %
-2 %
-8.0 %
-50.0 %
-31.0 %
-13 %
+16.0 %
-31.0 %
-2.0 %
+8 %
-4.0 %
-40.0 %
-36.0 %
-29 %
+21.0 %
-39.0 %
-34.0 %
-18 %
04:00 12:00 20:00
Time (UTC, HH:MM)
CO2 flux (µmolm−2s−1)

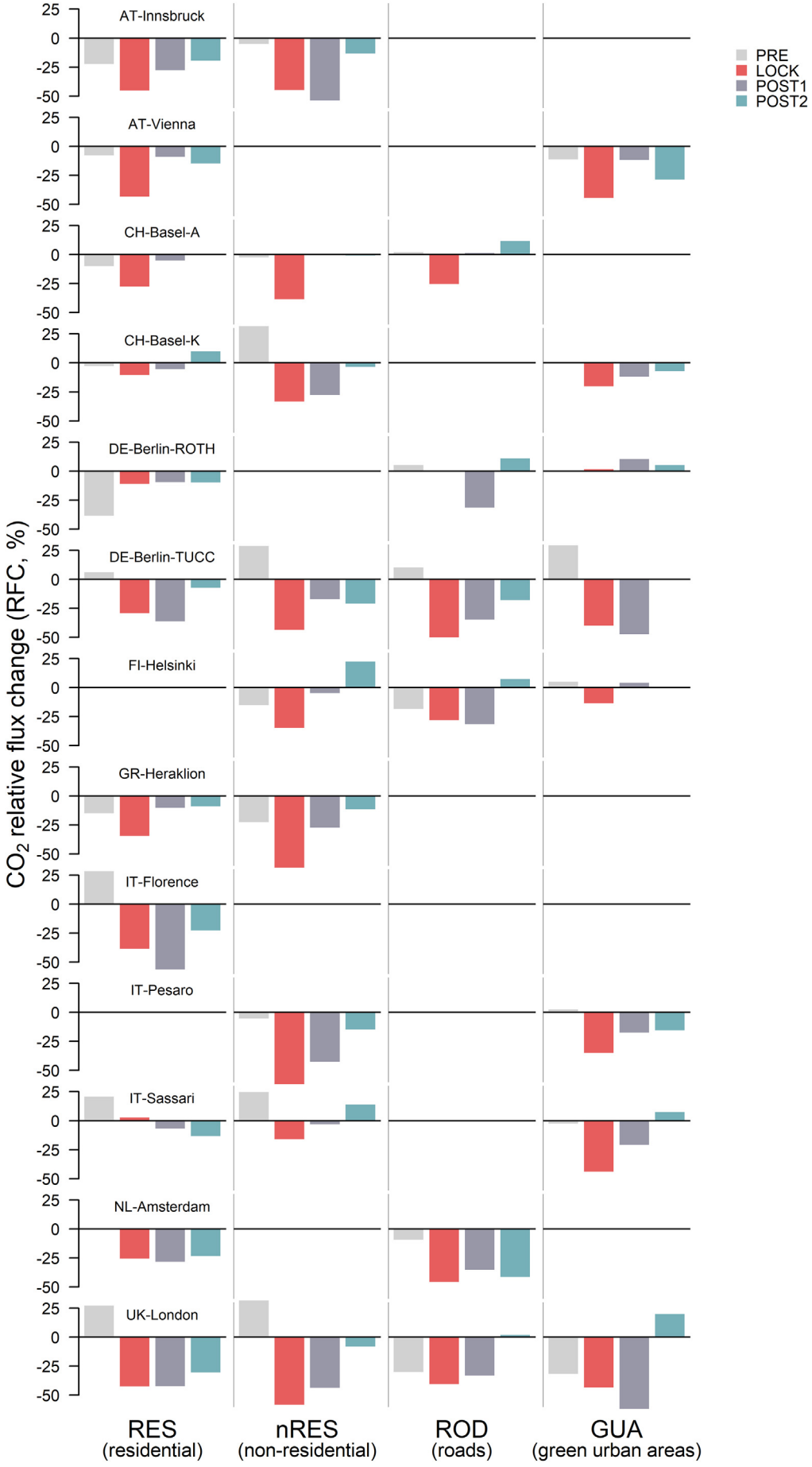
AT-Innsbruck
AT-Vienna
CH-Basel-A
CH-Basel-K
DE-Berlin-ROTH
DE-Berlin-TUCC
FI-Helsinki
GR-Heraklion
IT-Florence
IT-Pesaro
IT-Sassari
NL-Amsterdam
UK-London
25
0
-25
-50
PRE
LOCK
POST1
POST2
CO_2 relative flux change (RFC, %)
RES
(residential)
nRES
(non-residential)
ROD
(roads)
GUA
(green urban areas)

−36%, and decreased to −17% and − 7% in the POST1 and POST2 periods, respectively (star symbols in Fig. 3). In the period before the restriction or with SI < 20 (PRE, grey dots and stars in Fig. 3), the average *RFC* was not significantly different from zero.

3.3. Diel pattern of CO_2 fluxes

3.3.1. Effects of restrictions on diel CO_2 flux magnitudes

The analysis of diel CO_2 flux cycles established significant reductions in emissions in all districts during the LOCK period compared to each previous years (Table 2, LOCK period, min and max *RFC* values always negative), ranging from −10% at CH-Basel-K to −63% at GR-Heraklion. In all cases the reductions occurred mainly during daytime (Fig. 4), except for larger cities (AT-Vienna, NL-Amsterdam, UK-London), where restrictions had a clear effect also at night. Significant emission reductions during LOCK were observed at different hours of the day across districts, e.g. mainly in the morning at AT-Innsbruck and GR-Heraklion, and in the afternoon in CH-Basel-K and DE-Berlin-ROTH (Fig. 4).

During the PRE period, despite a natural interannual variability at all sites, emissions below the baseline values over previous years were already registered at AT-Innsbruck, CH-Basel-A and GR-Heraklion (Table 2, min and max always negative in the PRE period). This result is unlikely related to COVID-19 since no restrictions were in place for most of this period and the pandemic was not yet thought to have reached Europe. In Innsbruck and Basel, these lower than average emissions were attributed to especially warm temperatures in February 2020 (see Fig. S1). This likely caused a decrease in the use of domestic heating of which about 70% is by fossil fuel in Innsbruck and 25% in Basel. As a result, CO_2 emissions were reduced, in particular in the afternoon (Fig. 4, PRE column). In Heraklion, the temperature during this period was close to normal (supplementary "Air temperature analysis" section) and heating for this district is mainly from electricity. The reduction seen in early 2020 affected both the morning and afternoon peaks (Fig. 4 LOCK column), and this could be due to changes in the traffic regulations imposed by the city authorities in the city centre (Politakos et al., 2020).

The partial lifting of restrictions (periods POST1 and POST2) led to a general recovery of the emissions, which reached baseline levels during POST2 in 9 out of 13 districts (Table S8 for statistical analysis). In four cities (DE-Berlin-TUCC, IT-Pesaro, NL-Amsterdam and UK-London) emissions remained statistically lower during POST2, with *RFC* ranging between – 13% and −29% (see Fig. 4, POST2 column and Table S8 for statistical significance). At NL-Amsterdam the emissions remained below baseline level throughout the day (Fig. 4, last two columns), although social restrictions were not particularly stringent during POST2 (SI = 44.8, Table S2). However, this district is characterized by a strong presence of tourists, which the pandemic reduced drastically (Amsterdam saw a 60% reduction in tourism in July and August 2020, CBS Statistics Netherlands, 2021). This could also be the reason for the reductions observed at UK-London and IT-Pesaro during the POST periods. However, at UK-London, the restriction level remained high both during POST1 and POST2 (SI = 64.5 during POST2) compared to other cities, and the uptake of voluntary home-working was relatively high. These factors would also have contributed to keeping levels of socio-economic activities below the seasonal baseline in central London where the EC tower is located.

3.3.2. Effects of restrictions on diel CO_2 flux patterns

The diel patterns of the CO_2 fluxes in the different districts (Fig. 4) fall into two main categories: a bimodal emission pattern typical of districts with heavy traffic and accompanying rush-hour peaks (e.g. DE-Berlin-ROTH, GR-Heraklion, IT-Pesaro, IT-Sassari), and a monomodal pattern with a single maximum at midday (e.g. AT-Innsbruck, NL-Amsterdam and UK-London). At some sites the temporal pattern and the magnitude of the baseline fluxes remain similar over the different periods from PRE to POST2 (e.g. AT-Innsbruck, CH-Basel-A, GR-Heraklion, IT-Pesaro, compare grey lines in the four sub-plots per site in Fig. 4), while in other cases the flux magnitude and/or pattern changed over the different periods suggesting a seasonal change in the CO_2 fluxes, independently from the pandemic. For example at the IT-Florence site, fossil fuel combustion for building heating results in large emissions and hence large net CO_2 fluxes in winter. Later on in the year during POST1 and POST2 (late spring to summer), the magnitude of the emissions is substantially reduced and the two emission peaks seen in winter are replaced by a single peak around midday. This midday peak is related to emissions from traffic and commercial activities that in the centre of this touristic city are not characterized by commuter traffic (see also Fig. S7).

By comparing emissions from paired EC observations in residential and non-residential areas of the same city, it is possible to infer qualitative information on the dominant driver. For example, single peak emission patterns are observed at CH-Basel-A and DE-Berlin-TUCC, both sites dominated by non-residential areas (see Fig. S5) where emissions are more evenly distributed during the business hours. In contrast, bimodal emission patterns are seen at CH-Basel-K and DE-Berlin-ROTH, which are more representative of residential areas.

For most of these urban sites, the observed CO_2 fluxes are positive throughout the day and across the January to October period considered (Fig. 4). However, net CO_2 uptake was observed at DE-Berlin-ROTH and FI-Helsinki during POST1 and POST2, and attributed to vegetative drawdown. Potential confounding effects of vegetation drawdown on the analysis of net reductions in anthropogenic CO_2 emissions as a result of lockdown can be ruled out because the vegetation was not active during the PRE and LOCK periods (see the Vegetation Analysis section in the Supplement).

3.4. Role of urban features: land use type analysis

Wind sectors classified as non-residential areas (nRES) showed the largest emission reduction during the LOCK period in all cities (Fig. 5, second column red bars). The other land use types also showed reductions during LOCK in almost all districts, but those reductions persisted at least in part during the following POST1 and POST2 periods (recovery phase), while a quicker recovery of emission levels was experienced in nRES after starting POST1. The emissions recovery in residential areas (RES, Fig. 5 first column) was less clear, and followed different temporal dynamics across cities; this was likely due to pandemic-related changes in vehicular traffic, and emissions associated with domestic heating, cooking, and human respiration, which are functions of population density and other specific characteristics of each district. Similarly, sectors dominated by roads and green urban areas (ROD and GUA respectively, third and fourth column in Fig. 5) also showed site-specific emission dynamics during the recovery phase.

3.5. Comparison with city-scale activity data

Despite differences in spatial scales, there was a clear link between reductions in road traffic emissions estimated by the CM method using traffic congestion data (city scale), and lower measured CO_2 emissions in the ROD, RES and nRES sectors (neighbourhood scale) in all cities during LOCK (Fig. 6b, all points in the third quadrant). During the POST1 period (Fig. 6c), the correlation progressively decreased and disappeared during POST2 (Fig. 6d) when traffic emissions according to the CM are close to pre-pandemic levels. The negative *RFC* values still observed at many of the sites are thus thought to be related to other factors or specific local conditions. Similarly for the PRE period (Fig. 6a), as expected in the absence of mobility restrictions, no relationship was found between *RFC* and changes in traffic emissions.

Fig. 5. CO_2 relative flux change (*RFC*, %) as a function of the district's land use and lockdown period. For each period *RFC* was calculated for each half-hour and wind direction (2° bins) between CO_2 fluxes in 2020 and previous years and then averaged by sector. District sectors are defined as residential (RES), non-residential (nRES), roads, and green dominated (ROD and GUA respectively). Negative *RFC* means emission reduction.

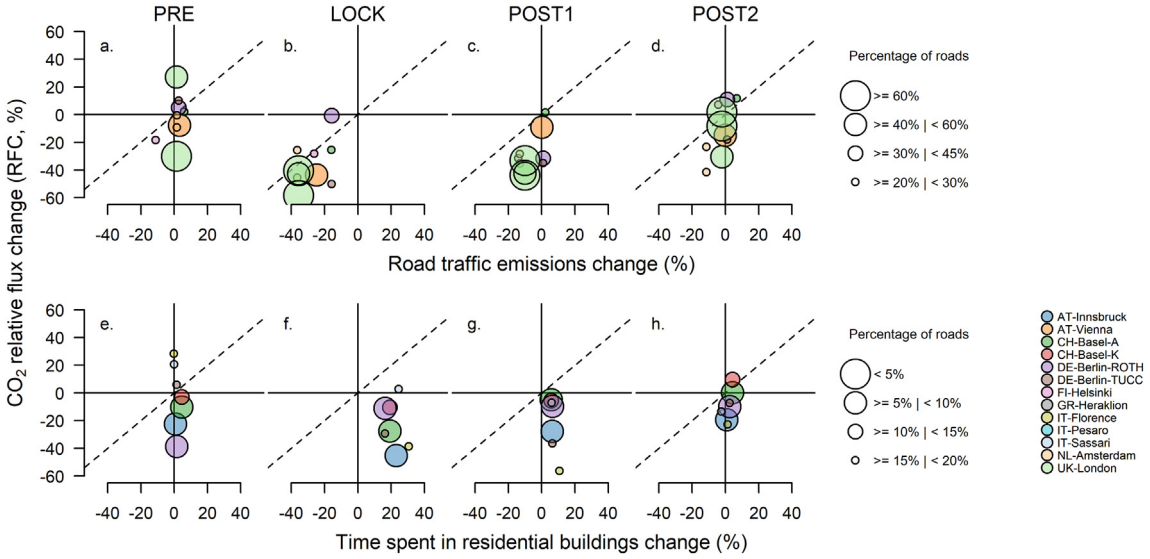

Fig. 6. Comparison of CO_2 relative flux change (*RFC*, %) and city-scale inventory data. Top panels (a–d): *RFCs* obtained from the EC flux measurements are compared against the road traffic emission change estimated using the Carbon Monitor (CM) modelling approach. *RFC* data used refer to district sectors covered mostly by residential buildings (RES), non-residential buildings (nRES), and roads (ROD). Data from sectors with less than 20% of roads were excluded from the analysis. Bottom panels (e–h.): *RFC* compared to the COVID-19 Google community mobility trends in residential areas (as average duration spent in places of residence). *RFC* data used refer to district sectors covered mostly by residential buildings, (RES), and having less than 20% of road coverage. The dashed lines represent 1:1 relationships. The comparison was done for the four COVID-19 periods (PRE, LOCK, POST1, POST2). As with *RFC* data, the daily city-scale emission estimates were smoothed using a 7-day rolling mean.

CO_2 emissions did not increase significantly in residential areas (with less than 20% of road cover) during the LOCK period, despite a mean 20% increase in time spent at home according to Google mobility data, and some instances of net reductions in emissions were recorded. This suggests that vehicular traffic is the main factor driving CO_2 fluxes in the monitored districts, with emissions from heating, cooking and human respiration playing a lesser role. The negative *RFC* in the three districts with less than 10% of roads during the PRE period (Fig. 6e, largest dots) could instead respond to a reduction in heating emissions due to anomaly warmer weather in these cities (e.g. Basel, Berlin, Innsbruck, see also Fig. 1 red lines and Fig. S1).

4. Conclusions

Direct CO_2 flux measurements from 13 eddy covariance (EC) stations across Europe reveal the effect of the COVID-19 pandemic restrictions on district level CO_2 emissions. At all sites, CO_2 emissions were significantly reduced during the strictest lockdown measures. In contrast to other approaches, the fine temporal resolution of EC data allows the evolution of the emissions to be analysed (at sub-daily to seasonal time-scales) and the changing response to restrictions to be quantified. For most sites CO_2 emissions returned to pre-pandemic levels by autumn of 2020. The emission reductions occurred mainly during daytime, principally as a consequence of limitations on mobility, and particularly reductions in vehicular traffic. In contrast, emissions related to home confinement (heating, cooking, human metabolism) did not increase enough to compensate for the reductions in emissions from road traffic; this was true in all neighbourhoods studied, even in the more residential ones where the workforce was displaced during lockdown periods.

The substantial emission reduction recorded through the first COVID-19 pandemic wave was temporary in most of the city districts and emissions rebounded to previous levels once restrictions were eased in the following months. The speed and extent of the emission recovery varied from district to district, with the fastest and most complete recovery seen mainly in the non-residential areas and attributed to re-established vehicular traffic.

This study demonstrates that the EC method is a valuable tool for monitoring continuously and almost in real-time the short- and long-term changes in urban trace gas emissions, and, potentially, for assessing the effectiveness of climate change mitigation policies (for example limiting traffic emissions versus reducing building heating demand). Of great importance to this aim is the availability of auxiliary data such as detailed traffic data, inventories of emission sources related to human activities, and data on city urban features. This study highlights the additional advantages of monitoring networks, where data collected from individual stations can be synergistically combined for long-term monitoring activities such as the Integrated Carbon Observation System (ICOS, www.icos-ri.eu).

Our results demonstrate that altering human behaviour has a direct, immediate and significant effect on the reduction and recovery of urban CO_2 emissions. The temporary nature of the observed emission reductions emphasises the need to implement systemic changes in the city ecosystem and people's lifestyles to achieve effective and sustained climate change mitigation. To reach the target of climate-neutrality in 2050, cities need to take action across multiple sectors but, according to our data, this must include interventions on private and public mobility aimed at reducing associated emissions.

CRediT authorship contribution statement

Giacomo Nicolini: Conceptualization, Methodology, Software, Formal analysis, Investigation, Writing - Original Draft. **Gabriele Antoniella**: Conceptualization, Data Curation, Investigation. **Federico Carotenuto**: Investigation, Writing - Review & Editing. **Andreas Christen**: Investigation, Writing - Review & Editing. **Philippe Ciais**: Investigation, Resources, Writing - Review & Editing. **Christian Feigenwinter**: Investigation, Writing - Review & Editing. **Beniamino Gioli**: Investigation, Writing - Review & Editing. **Stavros Stagakis**: Methodology, Investigation, Writing - Review & Editing. **Erik Velasco**: Methodology, Investigation, Writing - Review & Editing. **Roland Vogt**: Investigation, Writing - Review & Editing. **Helen C. Ward**: Methodology, Investigation, Writing - Review & Editing. **Janet Barlow**: Writing - Review & Editing. **Nektarios Chrysoulakis**: Investigation, Writing - Review & Editing. **Pierpaolo Duce**: Investigation, Writing - Review & Editing. **Martin Graus**: Investigation, Writing - Review & Editing. **Carole Helfter:** Investigation, Writing - Review & Editing. **Bert Heusinkveld**: Investigation, Writing - Review & Editing. **Leena Järvi**: Investigation, Writing - Review & Editing. **Thomas Karl**: Investigation, Writing - Review & Editing. **Serena Marras**: Investigation, Writing - Review &

Editing. **Valéry Masson**: Writing - Review & Editing. **Bradley Matthews**: Methodology, Investigation, Writing - Review & Editing. **Fred Meier**: Investigation, Writing - Review & Editing. **Eiko Nemitz**: Investigation, Writing - Review & Editing. **Simone Sabbatini**: Writing - Review & Editing. **Dieter Scherer:** Investigation, Writing - Review & Editing. **Helmut Schume**: Investigation, Writing - Review & Editing. **Costantino Sirca**: Investigation, Writing - Review & Editing. **Gert-Jan Steeneveld**: Methodology, Investigation, Writing - Review & Editing. **Carolina Vagnoli**: Writing - Review & Editing. **Yilong Wang**: Investigation, Writing - Review & Editing. **Alessandro Zaldei**: Investigation, Writing - Review & Editing. **Bo Zheng**: Investigation, Writing - Review & Editing. **Dario Papale**: Conceptualization**,** Methodology, Writing - Review & Editing, Validation, Supervision.

Data availability

All the eddy covariance datasets used in the study are available in Figshare under CC-BY licence (DOI: https://doi.org/10.6084/m9.figshare.13686292), together with the buildings and road traffic daily emissions as estimated by the CarbonMonitor method.

Other data that support the findings of this study are available at the following links:

- Oxford COVID-19 Government Response Tracker (OxCGRT) data are available at https://www.bsg.ox.ac.uk/research/research-projects/coronavirus-government-response-tracker#data
- Urban Atlas 2012 data are available at https://land.copernicus.eu/local/urban-atlas/urban-atlas-2012?tab=download
- Google Community Mobility Reports data are available at https://www.google.com/covid19/mobility/index.html?hl=en

Code availability

Data in this study were analysed using R (R Core Team, 2019) version 3.6.2 (2019-12-12, Dark and Stormy Night) and RStudio (RStudio Team, 2021) version 1.4.1717 (Juliet Rose). The custom code used for the analysis is available at: https://github.com/Giacomo-Nicolini/UrbanFluxes_COVID19.

Declaration of competing interest

The authors declare that they have no known competing financial interests or personal relationships that could have appeared to influence the work reported in this paper.

Acknowledgements

G.N. and S.Sa. thank the support of the ICOS Ecosystem Thematic Centre. G.A. thanks the support of the CHE H2020 Project (GA 776186). D.P. thanks the support of the "Departments of Excellence-2018" MIUR Program DIBAF "Landscape 4.0" and the CoCO2 H2020 (GA 958927) projects. G.J.S. acknowledges the funding from the Netherlands Organization for Scientific Research (NWO) VIDI grant "The Windy City" (file 864.14.007) and the funding from the Amsterdam Institute for Metropolitan Solutions for the AAMS observational network (Project VIR16002). L.J. acknowledges the Academy of Finland profiling action (grant number 311932) and CarboCity project (grant number 321527). FI-Helsinki is a station part of the ICOS network. N.C. thanks the support of the Municipality of Heraklion (Contract 105, 26/5/2020). F.M. and D.S. acknowledge the funding for instrumentation of the Urban Climate Observatory (UCO) Berlin from Deutsche Forschungsgemeinschaft (DFG) grant SCHE 750/8-1 and SCHE 750/9-1 of Research Unit 1736 "Urban Climate and Heat Stress in Mid-Latitude Cities in View of Climate Change (UCaHS)" and the research programme "Urban Climate Under Change ($[UC]^2$)", funded by the German Ministry of Research and Education (FKZ 01LP1602A). B.M. and H.S. acknowledge the funding from the City of Vienna (MA 7 – 596744/17) and the Vienna Science and Technology Fund (ESR20-030) as well as the support of A1 Telekom Austria in establishing and maintaining the measurement station at the A1 Arsenal tower. S.St. acknowledges funding from the European Union's Horizon 2020 research and innovation programme under the Marie Skłodowska-Curie grant agreement No 836443. E.N. and C.H acknowledge funding from the UK Natural Environment Research Council (NE/H003169/1, NE/K002279/1, NE/T001798/2) and thank the British Telecom for the access to the BT Tower and for supporting day-to-day activities. T.G.K., M.G. and H.C.W. acknowledge funding from the Austrian FWF (grant numbers P30600 and M2244).

Appendix A. Supplementary data

Supplementary data to this article can be found online at https://doi.org/10.1016/j.scitotenv.2022.154662.

References

Aubinet, M., Vesala, T., Papale, D., 2012. Eddy Covariance: A Practical Guide to Measurement and Data Analysis. Springer Netherlands, Dordrecht. https://doi.org/10.1007/978-94-007-2351-1.

Baldocchi, D., 2014. Measuring fluxes of trace gases and energy between ecosystems and the atmosphere - the state and future of the eddy covariance method. Glob. Chang. Biol. 20, 3600–3609. https://doi.org/10.1111/gcb.12649.

Christen, A., Coops, N.C., Crawford, B.R., Kellett, R., Liss, K.N., Olchovski, I., Tooke, T.R., Van Der Laan, M., Voogt, J.A., 2011. Validation of modeled carbon-dioxide emissions from an urban neighborhood with direct eddy-covariance measurements. Atmos. Environ. 45, 6057–6069. https://doi.org/10.1016/j.atmosenv.2011.07.040.

Crawford, B., Grimmond, C.S.B., Christen, A., 2011. Five years of carbon dioxide fluxes measurements in a highly vegetated suburban area. Atmos. Environ. 45, 896–905. https://doi.org/10.1016/j.atmosenv.2010.11.017.

Cross, M., Ng, S.K., Scuffham, P., 2020. Trading health for wealth: the effect of COVID-19 response stringency. Int. J. Environ. Res. Public Health 17, 1–15. https://doi.org/10.3390/ijerph17238725.

Feigenwinter, C., Vogt, R., Christen, A., 2012. Eddy covariance measurements over urban areas, Eddy covariance: a practical guide to measurement and data. Analysis, 377–397 https://doi.org/10.1007/978-94-007-2351-1.

Forster, P.M., Forster, H.I., Evans, M.J., Gidden, M.J., Jones, C.D., Keller, C.A., Lamboll, R.D., Quéré, C.Le, Rogelj, J., Rosen, D., Schleussner, C.F., Richardson, T.B., Smith, C.J., Turnock, S.T., 2020. Current and future global climate impacts resulting from COVID-19. Nat. Clim. Chang. 10, 913–919. https://doi.org/10.1038/s41558-020-0883-0.

Gioli, B., Toscano, P., Lugato, E., Matese, A., Miglietta, F., Zaldei, A., Vaccari, F.P., 2012. Methane and carbon dioxide fluxes and source partitioning in urban areas: the case study of Florence,Italy. Environ. Pollut. 164, 125–131. https://doi.org/10.1016/j.envpol.2012.01.019.

Goret, M., Masson, V., Schoetter, R., Moine, M.P., 2019. Inclusion of CO2 flux modelling in an urban canopy layer model and an evaluation over an old European city centre. Atmos. Environ. X 3, 100042. https://doi.org/10.1016/j.aeaoa.2019.100042.

Gualtieri, G., Brilli, L., Carotenuto, F., Vagnoli, C., Zaldei, A., Gioli, B., 2020. Quantifying road traffic impact on air quality in urban areas: a Covid19-induced lockdown analysis in Italy. Environ. Pollut. 267, 115682. https://doi.org/10.1016/j.envpol.2020.115682.

Gurney, K.R., Patarasuk, R., Liang, J., Song, Y., O'keeffe, D., Rao, P., Whetstone, J.R., Duren, R.M., Eldering, A., Miller, C., 2019. The Hestia fossil fuel CO2 emissions data product for the Los Angeles megacity (Hestia-LA). Earth Syst. Sci. Data 11, 1309–1335. https://doi.org/10.5194/essd-11-1309-2019.

Hale, T., Boby, T., Angrist, N., Cameron-Blake, E., Hallas, L., Kira, B., Majumdar, S., Petherick, A., Phillips, T., Tatlow, H., Webster, S., 2020. Variation in government responses to COVID-19, Version 9.0. Blavatnik Sch. Gov. Work. Pap.

Hale, T., Boby, T., Angrist, N., Cameron-Blake, E., Hallas, L., Kira, B., Majumdar, S., Petherick, A., Phillips, T., Tatlow, H., Webster, S., 2020. Oxford COVID-19 Government Response Tracker. Blavatnik Sch. Gov.

Helfter, C., Famulari, D., Phillips, G.J., Barlow, J.F., Wood, C.R., Grimmond, C.S.B., Nemitz, E., 2011. Controls of carbon dioxide concentrations and fluxes above central London. Atmos. Chem. Phys. 11, 1913–1928. https://doi.org/10.5194/acp-11-1913-2011.

Helfter, C., Tremper, A.H., Halios, C.H., Kotthaus, S., Bjorkegren, A., Grimmond, C.S.B., Barlow, J.F., Nemitz, E., 2016. Spatial and temporal variability of urban fluxes of methane, carbon monoxide and carbon dioxide above London, UK. Atmos. Chem. Phys. Discuss. 4, 1–31. https://doi.org/10.5194/acp-2016-216.

Järvi, L., Hannuniemi, H., Hussein, T., Junninen, H., Aalto, P.P., Hillamo, R., Mäkelä, T., Keronen, P., Siivola, E., Vesala, T., Kulmala, M., 2009. The urban measurement station SMEAR II: continuous monitoring of air pollution and surface-atmosphere interactions in Helsinki, Finland. Boreal Environ. Res. 14, 86–109.

Järvi, L., Nordbo, A., Junninen, H., Riikonen, A., Moilanen, J., Nikinmaa, E., Vesala, T., 2012. Seasonal and annual variation of carbon dioxide surface fluxes in Helsinki, Finland, in 2006–2010. Atmos. Chem. Phys. 12, 8475–8489. https://doi.org/10.5194/acp-12-8475-2012.

Jin, L., Schubert, S., Fenner, D., Meier, F., Schneider, C., 2020. Integration of a building energy model in an urban climate model and its application. Boundary-Layer Meteorol. https://doi.org/10.1007/s10546-020-00569-y.

Karl, T., Gohm, A., Rotach, M.W., Ward, H.C., Graus, M., Cede, A., Wohlfahrt, G., Hammerle, A., Haid, M., Tiefengraber, M., Lamprecht, C., Vergeiner, J., Kreuter, A., Wagner, J., Staudinger, M., 2020. Studying urban climate and air quality in the alps. Bull. Am. Meteorol. Soc. 101, E488–E507. https://doi.org/10.1175/BAMS-D-19-0270.1.

Kljun, N., Calanca, P., Rotach, M.W., Schmid, H.P., 2015. A simple two-dimensional parameterisation for flux footprint predictions FFP. Geosci. Model Dev. 8, 3695–3713. https://doi.org/10.5194/gmdd-8-6757-2015.

Lamprecht, C., Graus, M., Striednig, M., Stichaner, M., Karl, T., 2020. Decoupling of urban CO2 and air pollutant emission reductions during the European SARS-CoV2 lockdown. Atmos. Chem. Phys., 1–22 https://doi.org/10.5194/acp-2020-1080.

Le Quéré, C., Jackson, R.B., Jones, M.W., Smith, A.J.P., Abernethy, S., Andrew, R.M., De-gol, A.J., Willis, D.R., Shan, Y., Canadell, J.G., Friedlingstein, P., Creutzig, F., Peters, G.P., 2020. Temporary reduction in daily global CO2 emissions during the COVID-19 forced confinement. Nat. Clim. Chang., 1–8 https://doi.org/10.1038/s41558-020-0797-x.

Lietzke, B., Vogt, R., 2013. Variability of CO2 concentrations and fluxes in and above an urban street canyon. Atmos. Environ. 74, 60–72. https://doi.org/10.1016/j.atmosenv.2013.03.030.

Lietzke, B., Vogt, R., Feigenwinter, C., Parlow, E., 2015. On the controlling factors for the variability of carbon dioxide flux in a heterogeneous urban environment. Int. J. Climatol. 35, 3921–3941. https://doi.org/10.1002/joc.4255.

Liu, Z., Ciais, P., Deng, Z., Lei, R., Davis, S.J., Feng, S., Zheng, B., Cui, D., Dou, X., Zhu, B., Guo, Rui, Ke, P., Sun, T., Lu, C., He, P., Wang, Yuan, Yue, X., Wang, Yilong, Lei, Y., Zhou, H., Cai, Z., Wu, Y., Guo, Runtao, Han, T., Xue, J., Boucher, O., Boucher, E., Chevallier, F., Tanaka, K., Wei, Y., Zhong, H., Kang, C., Zhang, N., Chen, B., Xi, F., Liu, M., Bréon, F.-M., Lu, Y., Zhang, Q., Guan, D., Gong, P., Kammen, D.M., He, K., Schellnhuber, H.J., 2020. Near-real-time monitoring of global CO2 emissions reveals the effects of the COVID-19 pandemic. Nat. Commun. 11, 5172. https://doi.org/10.1038/s41467-020-18922-7.

Matese, A., Gioli, B., Vaccari, F.P., Zaldei, A., Miglietta, F., 2009. Carbon dioxide emissions of the city center of Firenze, Italy: measurement, evaluation, and source partitioning. J. Appl. Meteorol. Climatol. 48, 1940–1947. https://doi.org/10.1175/2009JAMC1945.1.

Matthews, B., Schume, H., 2022. Tall tower eddy covariance measurements of CO2 fluxes in Vienna,Austria. Atmos. Environ. 118941. https://doi.org/10.1016/j.atmosenv.2022.118941.

Matzarakis, A., Balafoutis, C., 2004. Heating degree-days over Greece as an index of energy consumption. Int. J. Climatol. 24, 1817–1828. https://doi.org/10.1002/joc.1107.

Montero, E., Van Wolvelaer, J., Garzón, A., 2014. The European urban atlas. In: Manakos, I., Braun, M. (Eds.), Land Use and Land Cover Mapping in Europe. Remote Sensing and Digital Image Processing. Springer, Dordrecht https://doi.org/10.1007/978-94-007-7969-3_8.

Nicolini, G., Antoniella, G., Carotenuto, F., Christen, A., Ciais, P., Feigenwinter, C., Gioli, B., Stagakis, S., Velasco, E., Vogt, R., Ward, H.C., Barlow, J., Chrysoulakis, N., Duce, P., Graus, M., Helfter, C., Heusinkveld, B., Järvi, L., Karl, T., Marras, S., Masson, V., Matthews, B., Meier, F., Nemitz, E., Sabbatini, S., Scherer, D., Schume, H., Sirca, C., Steeneveld, G., Vagnoli, C., Wang, Y., Zaldei, A., Zheng, B., Papale, P., 2022. URBAN_EC_COVID19_DATASET. Figshare data. [dataset] https://doi.org/10.6084/m9.figshare.13686292.

Nordbo, A., Järvi, L., Vesala, T., 2012. Revised eddy covariance flux calculation methodologies – effect on urban energy balance. Tellus B 64, 1–20. https://doi.org/10.3402/tellusb.v64i0.18184.

Oke, T.R., Mills, G., Christen, A., Voogt, J.A., 2017. Urban Climates. Cambridge University Press https://doi.org/10.1017/CBO9781107415324.004.

Pérez-Ruiz, E.R., Vivoni, E.R., Templeton, N.P., 2020. Urban land cover type determines the sensitivity of carbon dioxide fluxes to precipitation in Phoenix, Arizona. PLoS One 15, 1–26. https://doi.org/10.1371/journal.pone.0228537.

Pigeon, G., Legain, D., Durand, P., Masson, V., 2007. Anthropogenic heat release in an old European agglomeration (Toulouse, France). Int. J. Climatol. 27, 1969–1981. https://doi.org/10.1002/joc.1530.

Politakos, K., Stagakis, S., Chrysoulakis, N., 2020. Inter-annual variability of Eddy Covariance CO_2 flux measurements in the city center of Heraklion, Greece. ICOS Science Conference 2020, September 2020 https://doi.org/10.13140/RG.2.2.15867.34084.

R Core Team, 2019. R: a language and environment for statistical computing. URLR Foundation for Statistical Computing, Vienna, Austria. https://www.R-project.org/.

Ribeiro, H.V., Rybski, D., Kropp, J.P., 2019. Effects of changing population or density on urban carbon dioxide emissions. Nat. Commun. 10, 1–9. https://doi.org/10.1038/s41467-019-11184-y.

Roth, M., Jansson, C., Velasco, E., 2017. Multi-year energy balance and carbon dioxide fluxes over a residential neighbourhood in a tropical city. Int. J. Climatol. 37, 2679–2698. https://doi.org/10.1002/joc.4873.

RStudio Team, 2021. RStudio: Integrated Development Environment for R. URLRStudio, PBC, Boston, MA. http://www.rstudio.com/.

Salgueiro, V., Cerqueira, M., Monteiro, A., Alves, C., Rafael, S., Borrego, C., Pio, C., 2020. Annual and seasonal variability of greenhouse gases fluxes over coastal urban and suburban areas in Portugal: measurements and source partitioning. Atmos. Environ. 223. https://doi.org/10.1016/j.atmosenv.2019.117204.

Stagakis, S., Chrysoulakis, N., Spyridakis, N., Feigenwinter, C., Vogt, R., 2019. Eddy covariance measurements and source partitioning of CO2 emissions in an urban environment: application for Heraklion,Greece. Atmos. Environ. 201, 278–292. https://doi.org/10.1016/j.atmosenv.2019.01.009.

Staufer, J., Broquet, G., Bréon, F.M., Puygrenier, V., Chevallier, F., Xueref-Rémy, I., Dieudonné, E., Lopez, M., Schmidt, M., Ramonet, M., Perrussel, O., Lac, C., Wu, L., Ciais, P., 2016. The first 1-year-long estimate of the Paris region fossil fuel CO2 emissions based on atmospheric inversion. Atmos. Chem. Phys. 16, 14703–14726. https://doi.org/10.5194/acp-16-14703-2016.

Steeneveld, G.-J., van der Horst, S., Heusinkveld, B., 2020. Observing the surface radiation and energy balance, carbon dioxide and methane fluxes over the city centre of Amsterdam. EGU General Assembly 2020, Online, 4–8 May 2020, EGU2020-1547, pp. 3–4 https://doi.org/10.5194/egusphere-egu2020-1547.

Sugawara, H., Ishidoya, S., Terao, Y., Takane, Y., Kikegawa, Y., Nakajima, K., 2021. Anthropogenic CO2 emissions changes in an urban area of Tokyo, Japan, due to the COVID-19 pandemic: a case study during the state of emergency in April–May 2020. Geophys. Res. Lett. 48, 1–10. https://doi.org/10.1029/2021GL092600.

Turnbull, J.C., Karion, A., Davis, K.J., Lauvaux, T., Miles, N.L., Richardson, S.J., Sweeney, C., McKain, K., Lehman, S.J., Gurney, K.R., Patarasuk, R., Liang, J., Shepson, P.B., Heimburger, A., Harvey, R., Whetstone, J., 2019. Synthesis of urban CO2 emission estimates from multiple methods from the Indianapolis Flux Project (INFLUX). Environ. Sci. Technol. 53, 287–295. https://doi.org/10.1021/acs.est.8b05552.

Velasco, E., 2021. Impact of Singapore's COVID-19 confinement on atmospheric CO2 fluxes at neighborhood scale. Urban Clim. 37. https://doi.org/10.1016/j.uclim.2021.100822.

Velasco, E., Roth, M., 2010. Cities as net sources of CO2: review of atmospheric CO2 exchange in urban environments measured by eddy covariance technique. Geogr. Compass 4, 1238–1259. https://doi.org/10.1111/j.1749-8198.2010.00384.x.

Vogt, R., Christen, A., Rotach, M.W., Roth, M., Satyanarayana, A.N.V., 2006. Temporal dynamics of CO2 fluxes and profiles over a Central European city. Theor. Appl. Climatol. 84, 117–126. https://doi.org/10.1007/s00704-005-0149-9.

Vulova, S., Meier, F., Rocha, A.D., Quanz, J., Nouri, H., Kleinschmit, B., 2021. Modeling urban evapotranspiration using remote sensing, flux footprints, and artificial intelligence. Sci. Total Environ. 786. https://doi.org/10.1016/j.scitotenv.2021.147293.

Ward, H.C., Kotthaus, S., Grimmond, C.S.B., Bjorkegren, A., Wilkinson, M., Morrison, W.T.J., Evans, J.G., Morison, J.I.L., Iamarino, M., 2015. Effects of urban density on carbon dioxide exchanges: observations of dense urban, suburban and woodland areas of southern England. Environ. Pollut. 198, 186–200. https://doi.org/10.1016/j.envpol.2014.12.031.

Yadav, V., Ghosh, S., Mueller, K., Karion, A., Roest, G., Gourdji, S.M., Lopez-Coto, I., Gurney, K.R., Parazoo, N., Verhulst, K.R., Kim, J., Prinzivalli, S., Fain, C., Nehrkorn, T., Mountain, M., Keeling, R.F., Weiss, R.F., Duren, R., Miller, C.E., Whetstone, J., 2021. The impact of COVID-19 on CO2 emissions in the Los Angeles and Washington DC/Baltimore metropolitan areas. Geophys. Res. Lett. 48, 1–10. https://doi.org/10.1029/2021gl092744.